INTERNATIONAL JOURNAL OF ADVANCED ROBOTIC SYSTEMS

International Journal of Advanced Robotic Systems
July-August 2020: 1–8

DOI: 10.1177/1729881420916963
journals.sagepub.com/home/arx
SAGE

Development and application of a temperature gradient detector for manned underwater robot

Dewei Li[1,2], Ye Li[1], Zhongjun Ding[2], Xiangxin Wang[2] and Baohua Liu[2]

Abstract

Manned underwater robot is an important platform to carry various sensors and working tools to finish the in situ measurement and sampling in the deep sea. Due to its limited loading capacity, the device it will be carried, usually, requires to be able to dive to its working depth with a small volume and weight. According to the application requirements of deep-sea sediment temperature gradient in situ measurement observed, a detector system that can obtain data in situ is designed, which mainly includes a titanium alloy electronic cabin and a temperature probe. A comprehensive design analysis method is used to compare and analyze the ultimate static pressure, stability limit load, bending moment load, and transient temperature field on the underwater operation conditions. Optimal dimensions and filled media in the probe are decided. Finally, the pressure resistance test is finished in the lab, and scientific application is conducted on Jiaolong's 127th dive in the Northwest Indian Ocean, which successfully sampling the temperature gradient data of deep-sea sediments in the Daxi hydrothermal area. The method introduced in this article can effectively improve the safety and reliability of deep-sea structure and greatly reduce costs throughout the design cycle.

Keywords

Manned underwater robot, temperature gradient, ANSYS simulation, in-situ measurement, pressure resistance test

Date received: 30 January 2020; accepted: 25 February 2020

Topic Area: Field Robotics
Topic Editor: Yangquan Chen
Associate Editor: Xiao Liang

Introduction

The temperature gradient of seabed sediments is an important parameter to describe the thermal state of seabed sediments, which is of great significance to study the internal energy transfer, deep thermal state, thermal evolution, and deep-sea resource distribution of the earth.[1–5] An additional function is for establishing heat flow, which is a vital component of calculating thickness of the gas hydrate stability zone.

The submarine temperature gradient is normally detected by inserting a slender metal cylinder equipped with temperature sensors into the seafloor sediment during operation. There are well-established methods for detecting the temperature gradient. Bullard designed a geothermal probe with the thermistor in a thin steel pipe to measure the in-situ temperature and geothermal gradient in the Pacific Ocean,[6] the effect of frictional heat generated during the initial insertion of the probe by increasing the

[1] Shipbuilding Engineering College, Harbin Engineering University, Harbin, China
[2] Technology Department, National Deep Sea Center, Qingdao, China

Corresponding author:
Ye Li, Shipbuilding Engineering College, Harbin Engineering University, Harbin 150000, China.
Email: ldw@ndsc.org.cn

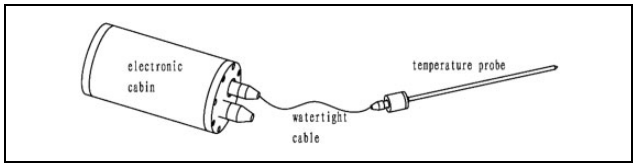

Figure 1. Structure design of the temperature gradiometer.

measurement time. Another important method designed by Ewing was to install the thermistor inside a stainless steel tube which was mounted 1 cm away from the wall of the piston corer.[7] The advantages of this method are fast response, short measurement time, and strong penetrating ability. It can penetrate the meters with a piston corer, and the data could be obtained less than 10 min, and the parameters of $\nabla T/\nabla Z$ and K could be measured in the same position. An alternative method to measure the thermal conductivity in situ was proposed by Lister[8] to use the heat pulse, and careful analysis of this method was illustrated by Lister in 1979.[9]

Due to the complexity of the deep-sea bottom environment and the instability of ship movements on the surface, some probe was designed and tested to measure the temperature gradient operated by remotely operated vehicles (ROVs)[10–13] but not which in research vessel. Both of the methods mentioned above were affected by the angle and movement of the probe for the reasons of long-distance operation. So, the stable and accurate in situ measurement should be very important for the in-situ measurement of the submarine temperature gradient.

The greatest character of manned underwater robot is their ability to allow scientists to carry out the survey and research in the deep sea.[14] In this article, a deep-sea temperature gradient detector was designed as a working tool of Jiaolong manned underwater robot to obtain the in situ temperature gradient of deep-sea cold spring and sediment.

In the following, we describe the design of the new device and evaluate the heat transfer and structural reliability of the detector using numerical simulations method. In addition, the device was operated by Jiaolong manned underwater robot on its 127 dive during the cruise of R/V Xianghong 09 in 2017.

Construction and capabilities

The core components of this detector are an electronic compressive cabin and a temperature probe (Figure 1). On the stage of preparation, the electronic compressive cabin is fixedly installed in the underwater robot sampling basket, and the temperature probe is placed on the sampling basket, two components are connected by a watertight cable. When Jiaolong dive to the seabed, the temperature probe was operated by manipulator to insert the sediment to detect the temperature gradient. For its small size and lightweight, the operation of temperature gradient sampling became simplified and the data are more accurate.

To satisfy the working depth of 7000 m, the TC4 was selected as the manufacturing material to ensure that the structure is both mechanically robust and relatively inert to galvanic corrosion in seawater. The safety coefficient was set at 1.11, and the pressure was calculated at 78 MPa.[15,16] In temperature probe, three NTC sensors are glued each into one 4-mm long brass cylinder with a diameter of 4 mm at an even spacing of 200 mm. A pointed tip and a compressive cabin are welded at the lower and the top of the probe. Electrical wires connect the sensors to a Sub-Conn connector, which were installed at the end of the compressive cap, the temperature information was collected and processed in the electronic cabin, and then fed back to the manned cabin so that the scientists could observe temperature changes in-situ. Before closing the compressive cabin on the top of the probe, the ISOPAR M oil was filled to minimize disturbances of the temperature profiles along the probe.

Mechanical design

Electronic cabin

According to the scientists' need for in-situ temperature detection, control and detection circuits are fixed in the electronic compressive cabin. The control circuit includes a microcomputer control system and a 12-channel data acquisition circuit with flash and SD memory functions. The detection circuit includes a precision bridge system, a power control system, a precision voltage reference system, and a signal conditioning circuit. The electronic compressive cabin here is a short cylinder, the inner diameter used for installing circuit systems is 110 mm, and the thickness of the cabin is estimated by

$$s_2 \approx D\left(\frac{mpL}{2.6\,ED}\right)^{0.4} \tag{1}$$

and maximum critical pressure of the cabin could be calculated by

$$P_k = 2.6E\frac{(S/D)^{2.5}}{L/D} \tag{2}$$

where m is the safety factor of 2, p is the design pressure of 78 MPa, L is the length of the cabin of 240 mm, and E is the elastic modulus (MPa) of TC4. So, the thickness and the critical pressure of the cabin are 9 mm and 250.99 MPa.

Temperature probe

The probe is the main tool for measuring the temperature gradient of deep-sea sediments. It is designed that firstly, it should be operated by manipulator conveniently, secondly, it should have the ability to work on the high-pressure condition with stability, so that not easy to deform during the process of inserting the probe into the sediment.

Stability calculation of external pressure

Different from the probe of Lister and Ewing,[17] the temperature probe operated by manipulator should be small and light, for the less weight and higher strength, the TC4 was used for designing the probe. The inner diameter of the probe is 10 mm and the length of the probe is 600 mm. For the probe with a compressive cabin and a long cylinder, thickness of the probe is estimated to be 2 mm and maximum critical pressure of the probe could be calculated by

$$P_k = \frac{2E}{1-\mu^2}\left(\frac{S}{D}\right)^3 \tag{3}$$

where S is the probe thickness, D is the middle diameter, μ is 0.3 for the TC4. According to the parameters given above, the critical pressure of the probe is 1119.25 MPa, which is 14 times of the design pressure 78 MPa.

Stability calculation of compressive rod

Based on the material mechanics stabilizing principle of rods, the critical load of equal section with different constraints is calculated by

$$F_{cr} = \frac{\pi^2 IE}{(\mu l)^2} \tag{4}$$

The F_{cr} was calculated when

$$\lambda > \lambda_p \tag{5}$$

where probe flexibility $\lambda = \mu l / i_{\min}$, and minimum inertia radius $i_{\min} = \sqrt{I_{\min}/A} = 4.29 \times 10^{-3}$ m, so $\lambda = 97.9$, and ultimate flexibility of TC4 $\lambda_p = \sqrt{\pi^2 E/\sigma_P} = 38.49$. E is the elastic modulus (MPa) with 1.1×10^5 of TC4; I is the moment of inertia in bending (m^4), $I = \frac{\pi}{64}\left(D^4 - d^4\right) = 1.39 \times 10^{-9}$ with D of 0.014 m and d of 0.01 m; μ is the length coefficient of 0.7 for a pressure fixed at one end and twisted at the other end; and l is the length of the probe (m) of 0.6 m. F_{cr} is theoretically calculated of $8546.1N$.

Finally, the thickness of electronic compressive cabin was determined by 9 mm with inner diameter and length of 110 and 240 mm, and the thickness of temperature probe was determined by 2 mm with inner diameter and length of 10 and 600 mm.

Numerical simulation

The main failure of cylinder chamber under the external pressure is strength failure and buckling failure; after theoretical calculation, the static structural and buckling model of electronic cabin and temperature probe is numerically simulated. Meantime, due to the precious time of manned underwater robot when working under the sea, transient heat transfer analysis with different intermediary substance is also simulated.

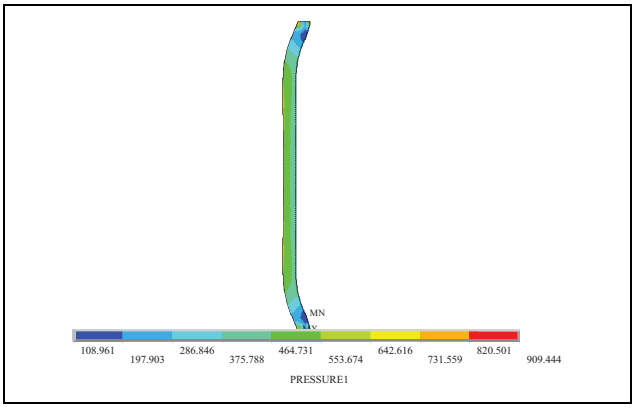

Figure 2. Stress distribution.

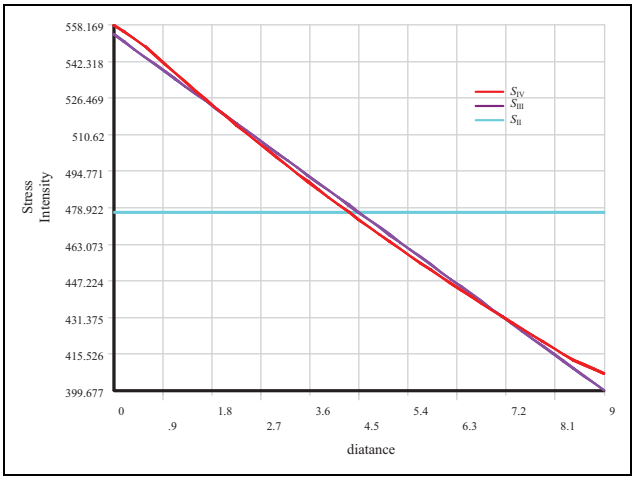

Figure 3. Result of equivalent linearization.

Strength simulation

For the external pressure cylinder, in addition to designing and checking its stability, the compressive stress of the cylinder inner wall should also be checked and the pressure in the inner wall should not exceed the yield baseline at the material design temperature.

The model of the electronic cabin and temperature probe is molding in the ANSYS, for the electronic cabin, the thickness varying from 1 mm to 15 mm is chosen to simulate the intensity variable along the inner wall. During the simulation, the material of TC4 which maximum yield strength of 825 MPa is used, the quadrangle grids are utilized.

Degrees of freedom in both two sides of the cylinder are fixed, the 78 MPa pressure is loaded on the outside of the surface. The evaluation lines at the dangerous section are chosen, and the equivalent linearization method is used to decompose various stresses on the evaluation line into film stress, bending stress, and peak stress. Results at the length of 240 mm and thickness of 9 mm are shown in Figures 2 and 3 below, general primary membrane stress is 476.8 MPa, less than the safe allowable stress 705 MPa.

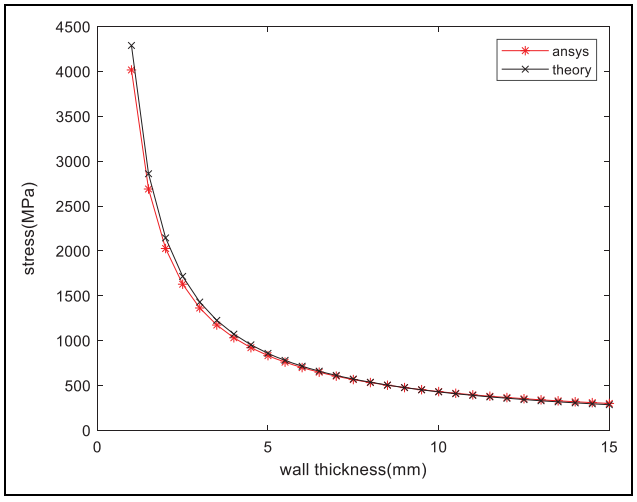

Figure 4. Comparison of ANSYS and theory results.

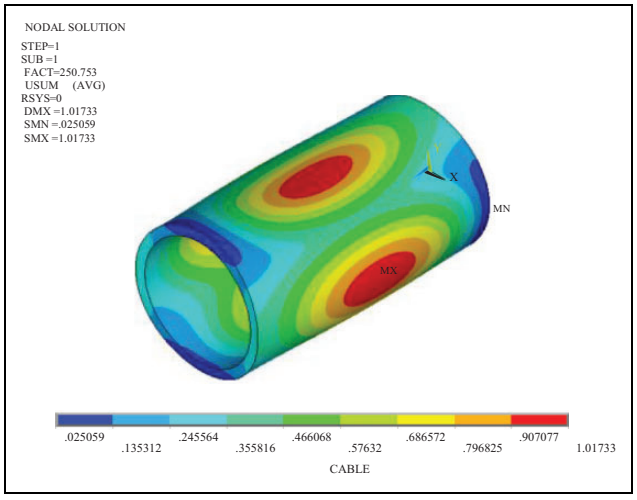

Figure 6. Buckling analysis of cabin.

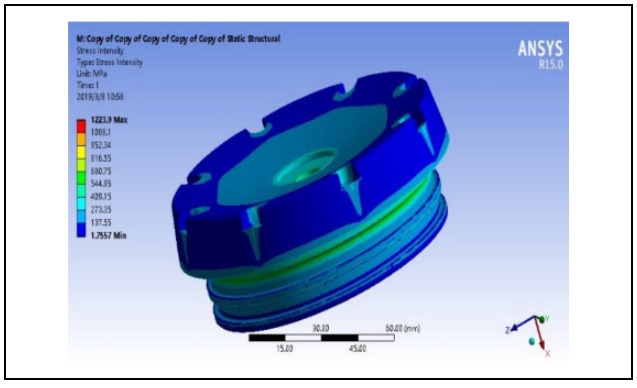

Figure 5. Stress analysis of cap.

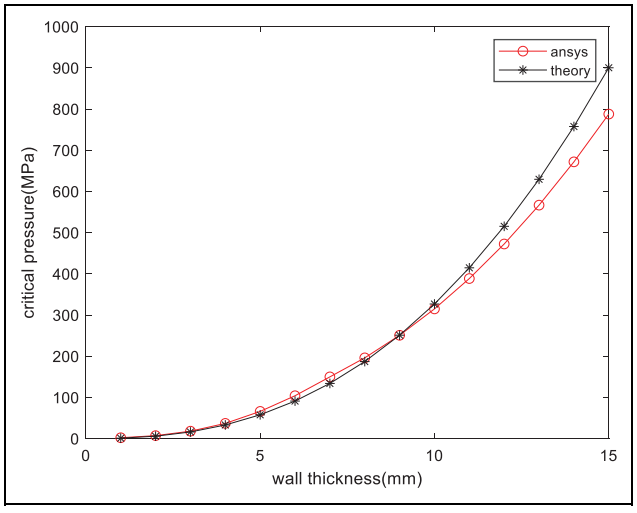

Figure 7. Critical pressure comparison with various wall thickness.

The results compared between ANSYS and theory are shown in Figure 4, related errors between the results of ANSYS simulation and theory calculation are within 0.049%–6.7%, and the stress intensity is decreased as the wall thickness increased. Minimal error 0.049% is obtained at the thickness of 9 mm. Besides, the stress analysis of cap is shown in Figure 5, in which maximum strain under 78 MPa pressure is 0.15 mm and maximum stress is 1223.9 MPa with safety factor of 1.5.

Stability simulation

Pressure vessels often generate compressive stress in the whole or local area due to mechanical or thermal load and may cause the overall or local instability of the structure. The instability of a cylindrical container under external pressure is usually a waveform that changes its cross section, but the number of waveforms is related to the thickness or length of the cylinder.

Because of the dimension of circuit systems, the inner diameter of 110 mm is required, so the stability simulations are carried out to find the optimal dimension. The buckling analysis results on the thickness of 9 mm and length of 240 mm are shown in Figure 6, the number of circumferential waveforms in buckling instability is 2, and critical pressure is 250.753 MPa compared with 250.99 MPa theoretical results.

Additionally, considering the initial defects of the geometry, serious nonlinear buckling analysis is conducted to find the optimal dimension. The maximum critical pressure compared between theory results and ANSYS simulation results when cabin length is 240 mm and wall thickness increase from 1 mm to 15 mm is shown in Figure 7, errors decrease from 50% to 0.098% with wall thickness increase from 1 mm to 9 mm, and then increased up to −14.27% when wall thickness is 15 mm. Meantime, the comparison results when wall thickness is 9 mm and cabin length increase from 230 mm to 250 mm are shown in Figure 8, errors decrease from 3.9% to 0.098% with length increase from 230 mm to 240 mm, and then increased up to −3.7% when cabin length is 250 mm.

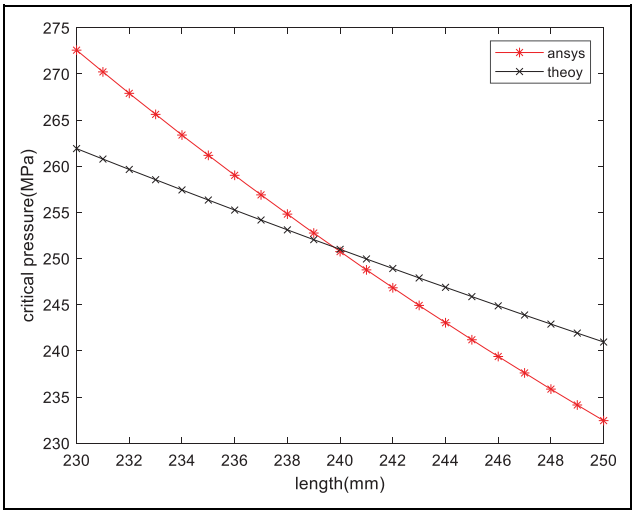

Figure 8. Critical pressure comparison with various length.

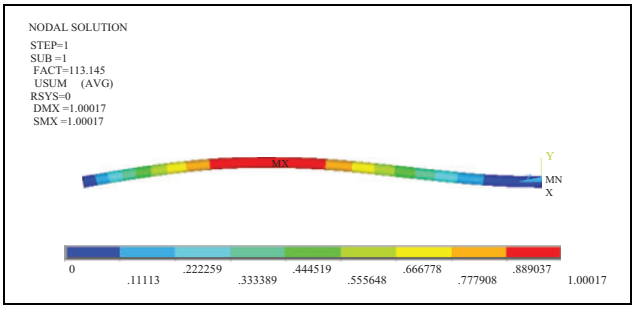

Figure 9. Stability analysis of compressive rod.

Stability analysis of compressive rod is also finished and the ultimate pressure of the cross section is 113.145 MPa in Figure 9, and the ultimate force of F_{cr} is obtained with 8526.6 N, which is approximately equal to the theoretical results calculated above.

Transient temperature simulation

For the precious time of manned underwater robot working under the sea, sampling time of the temperature probe should be as soon as possible, so the thermal equilibrium inside the probe field could be reached in a short time. In this section, three typical media conditions are used to simulate the transient temperature field when thermal equilibrium reached.

The simplified axisymmetric geometry model is shown in Figure 10, three NTC temperature sensors are glued each into a 4-mm long brass cylinder with a diameter of 4 mm, the space of each sensor is 200 mm. Air, sand, and ISOPAR M oil are selected as the media in the probe to analyze the temperature change; all parameters used to define the numerical model are listed in Table 1.

Assume the temperature of the sensor before underwater robot diving is 18°C and the temperature of the deep

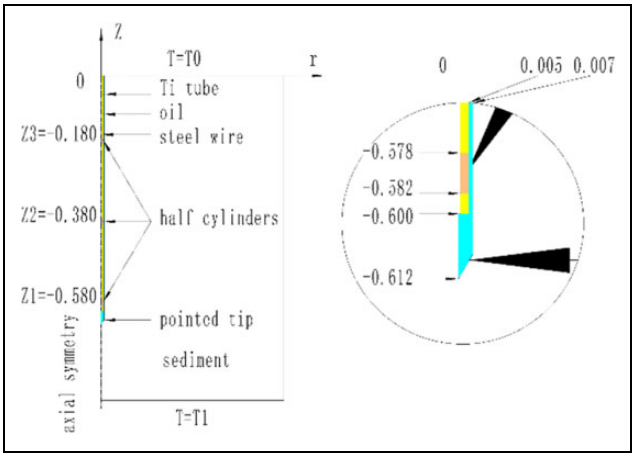

Figure 10. Geometry model of the probe.

Table 1. Parameters of the numerical model.

Constant	Description	Value
k_{TC4}	Thermal conductivity of TC4	6.7 W/(m K)
c_{TC4}	Specific heat of TC4	526.3 J/(kg K)
ρ_{TC4}	Density of TC4	4510 kg/m^3
k_{sand}	Thermal conductivity of sand	0.225 W/(m K)
c_{sand}	Specific heat of sand	920 J/(kg K)
ρ_{sand}	Density of sand	2650 kg/m^3
k_{oil}	Thermal conductivity of oil	0.121 W/(m K)
c_{oil}	Specific heat of oil	199 J/(kg K)
ρ_{oil}	Density of oil	790 kg/m^3
k_{air}	Thermal conductivity of air	0.02389 W/(m K)
c_{air}	Specific heat of air	1009 J/(kg K)
ρ_{air}	Density of air	1.243 kg/m^3
k_{brass}	Thermal conductivity of brass	71 W/(m K)
c_{brass}	Specific heat of brass	394 J/(kg K)
ρ_{brass}	Density of brass	8410 kg/m^3

seawater is 1.8°C, the convection coefficient of seawater is 454.24 W/(m^2 K), and the media flow in the probe ignored.The model consisted of 4782 finite elements, axisymmetric constraints are loaded at the center of the probe, initial temperature of 18°C is added on the surface of three sensors and medium, and the thermal equilibrium temperature of 1.8°C is added on the external surface of the probe. Transient temperature comparison is shown in Figure 11. Different media such as oil, sand, and air reach equilibrium respectively at 812, 1428.6, and 3456.9 s (errors in 1‰). Comparison at the time of 900 s is shown in Figure 12, and temperature of the sensor is 1.844°C and 3.125°C separately. To evaluate and compare the times required for the probe to reach thermal equilibrium after insertion into the sediment, conditions when temperature on the probe external surface from 1.779°C to 1.783°C in 900s are also simulated and results are shown in Figure 13. When medium is oil, 470 s is sufficient to finish the sampling, but when medium is sand or air, 830 or 2370 s is needed.

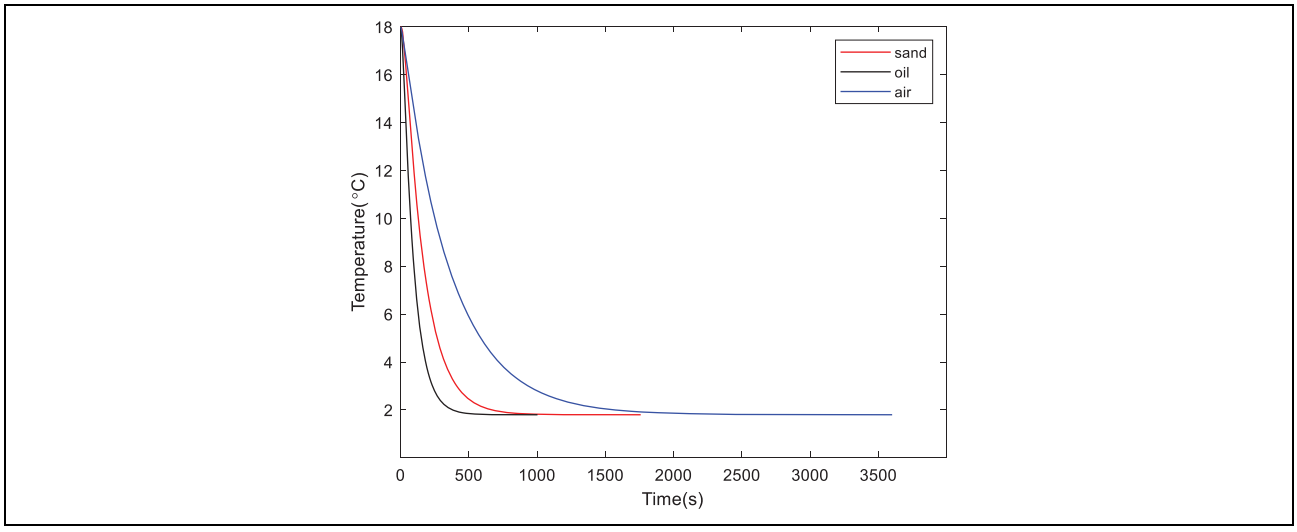

Figure 11. Transient temperature comparison.

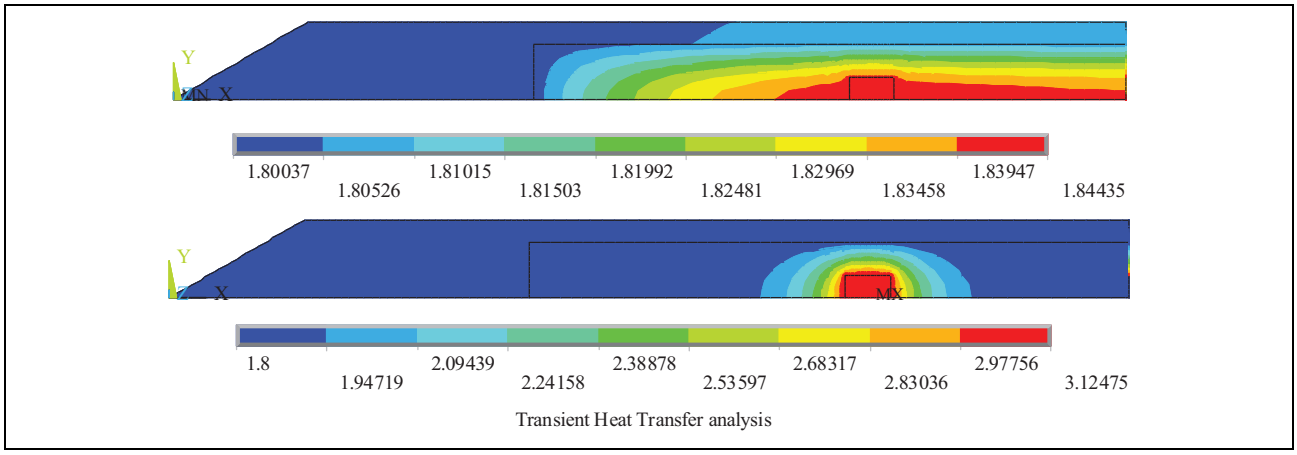

Figure 12. Comparison of temperature field at 900 s (sand and air).

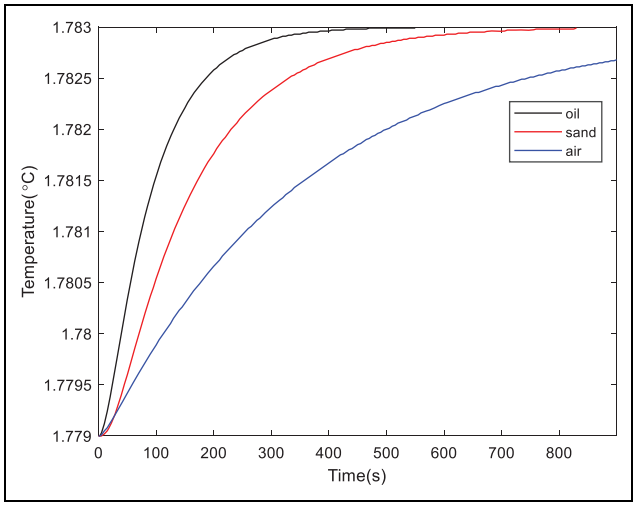

Figure 13. Simulation of sampling process.

Figure 14. Package of the detector.

From simulation analysis above, ISOPAR M oil is the optimal material to be filled into the probe as medium, and sampling time when inserting the probe into the sediment just needs to be longer than 10 min.

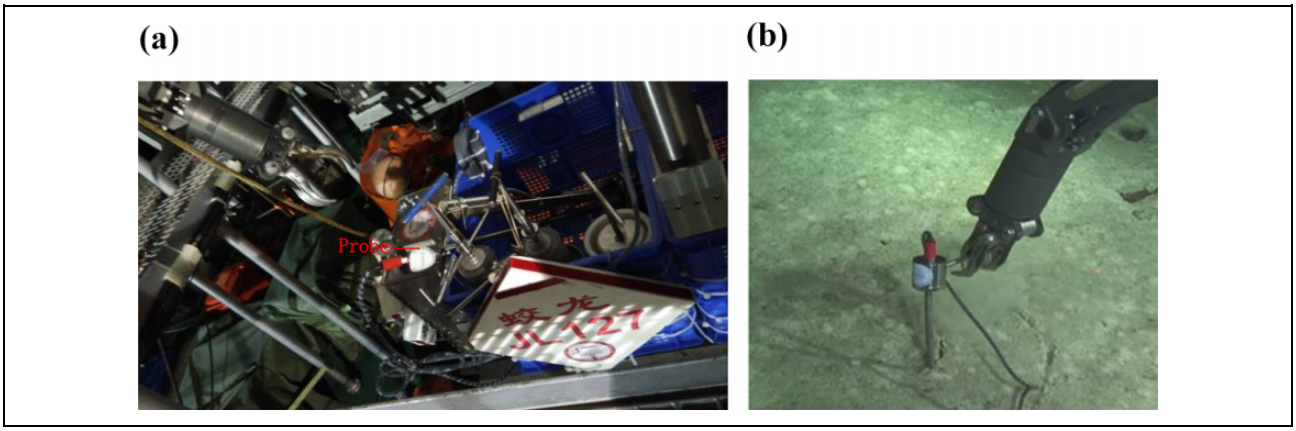

Figure 15. (a) Installed and (b) operated by Jiaolong.

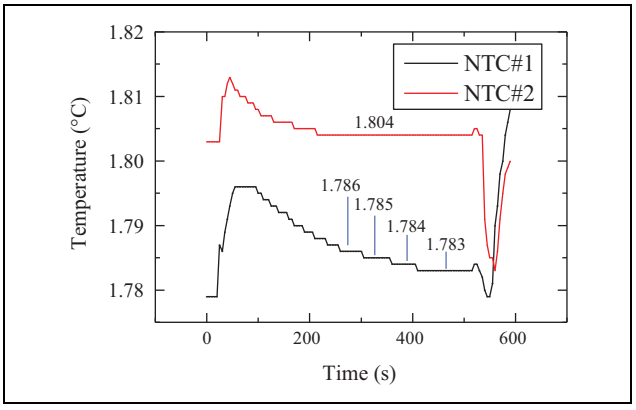

Figure 16. Experimental data.

Pressure test and application

To test the stability of the electronic cabin and probe designed above, deep-sea high-pressure simulation system is used to conduct pressure resistance test. The package of detector is shown in Figure 14. The maximum test pressure is set up to 78 MPa, which is 1.11 times of the working pressure. Pressure added in steps of 2.5 MPa/min and then kept 3 min at every increase of 10 MPa, until pressure increased up to 78 MPa, and 6 h is hold to check the stability. Finally, pressure gradually reduced in steps of 1.25 MPa/min until the standard atmospheric pressure achieved.

On the process of test, no pressure leakage happened and after the systems taken out, no obvious deformation found, indicating that the probe and electronic cabin structure are safe to install on the basket of the Jiaolong manned underwater robot.

The deep-sea temperature gradient detector was used on the 127 dives of Jiaolong to carry out scientific investigation in the Northwest Indian Ocean with a depth of 3400 m. The layout of the system installed in sampling basket and the operation diagram recorded by HD camera are shown in Figure 15. Due to the shallow sediment coverage in the operation area, only NTC #1 and NTC #2 completely entered the sediment.

Data of sensors when inserting the probe into the sediment are shown in Figure 16. At the first stage of inserting the probe into the sediment, temperature rises about 0.02°C due to the friction heating effect, and then temperature begins to decline until sediment environment temperature and probe temperature reach equilibrium with resolution temperature change of 0.001°C. The time for the whole process is about 450 s, which verifies the effectiveness of the simulation above.

Conclusions

In this research, a kind of deep-sea temperature gradient detector that could be installed on Jiaolong manned underwater robot is developed. Various operation conditions are conducted on the geometry model to verify the structure strength and buckling stability, and then three different media are used to simulate the time it takes for the temperature probe to reach thermal equilibrium when it is operated under the sea.

Pressure resistance test and scientific application carried out by Jiaolong are completed. The results show that the system has successfully obtained the temperature gradient data of the deep-sea sediments in the Northwest Indian Ocean, which verifies the significance of the comprehensive design and simulation analysis method for undersea working tools.

Declaration of conflicting interests

The author(s) declared no potential conflicts of interest with respect to the research, authorship, and/or publication of this article.

Funding

The author(s) disclosed the following financial support for the research, authorship, and/or publication of this article: This work was supported by the "National Key R&D Program of China" (2017YFC0306600, 2016YFC0302600, 2016YFC1401300).

ORCID iD

Dewei Li https://orcid.org/0000-0002-0148-1382

References

1. Zhongjun D, Baohua L and Zhongchen L. Research on multi-function in-situ detect miniature probe of sea sediment. *J Electron Measure Instrum* 2009; 23(12): 44–48.
2. Yu Z and Shengwe Z. A design of high accurate temperature measuring system based on platinum resistance transducers. *Chin J Sensors Actuators* 2010; 23(3): 311–314.
3. Feng ZT, Jia-Jun L and Mo L. Design and realization of temperature measurement circuit of miniature boomerang seafloor sediment heat-flow probe. *J Ocean Technol* 2017; 6: 44–48.
4. Pfender M and Villinger H. Miniaturized data loggers for deep sea sediment temperature gradient measurements. *Mar Geol* 2002; 186 (3): 557–570.
5. Chang HI and Shyu CT. Compact high-resolution temperature loggers for measuring the thermal gradients of marine sediments. *Mar Geophys Res* 2011; 32(4): 465–479.
6. Bullard EC. The flow of heat through the floor of the Atlantic Ocean. *Proc R Soc London, A* 1954; 222: 408–429.
7. Gerard R, Langseth MG Jr and Ewing M. Thermal gradient measurements in the water and bottom sediments of the Western Atlantic. *J Geophys Res* 1962; 67: 785–803.
8. Lister CRB. Measurement of in situ sediment conductivity by means of a Bullard-type probe. *Geophys J R Astron Soc* 1970; 19: 521–532.
9. Lister CRB. The pulse-probe method of conductivity measurement. *Geophys J R Astron Soc* 1979; 57: 451–461.
10. Feseker T, Dählmann A, Foucher J-P, et al. In-situ sediment temperature measurements and geochemical porewater data suggest highly dynamic fluid flow at Isis mud volcano, eastern Mediterranean Sea. *Mar Geol* 2009; 261(1–4): 128–137.
11. Treude T, Reischke S, Feseker T, et al. Microbial methane oxidation and chemoauthotrophic communities at the North Alex mud volcano, Eastern Mediterranean. *Geophys Res Abs* 2009; 11, EGU 2009-11025.
12. Feseker T, Wetzel G and Heesemann B. Introducing the T-Stick: a new device for high precision in situ sediment temperature profile measurements. *Limnol Oceanogr Meth* 2012; 10(1): 31–40.
13. Kang-Kang L, Huai T, Mingya X, et al. Design for deep sea vehicle dedicated heat flow probes. *Transducer Microsyst Technol* 2014; 09: 62–64+67.
14. Feng L. Technical status and development trend of the deep-sea manned underwater robot. *J Eng Stud* 2016; 8(2): 172–178.
15. Dewei L, Zhongjun D, Yugang R, et al. Design and experimental study on deep-sea bucket foundation installation equipment. *China Mech Eng* 2018; 493(13): 60–65.
16. Zhian Z, Huajie Y and Xinli W. *Chemical equipment design foundation*. Beijing: Chemical Industry Press, 2001, p. 206.
17. Lewis TJ, Villinger H and Davis EE. Thermal conductivity measurements of rock fragments using a pulsed needle probe. *Can J Earth Sci* 1993; 30: 480–485.